Eddy mean flow decomposition and eddy diffusivity estimates in the tropical Pacific Ocean: 2. Results

S. Bauer

Atlantic Oceanographic and Meteorological Laboratory, National Oceanic and Atmospheric Administration, Miami, Florida, USA

M. S. Swenson

Fleet Numerical Meteorology and Oceanography Center, Monterey, California, USA

A. Griffa

Istituto Studio Oceanografia Fisica, Consiglio Nazionale Ricerche, La Spezia, Italy

Received 25 August 2000; revised 12 February 2002; accepted 10 May 2002; published 16 October 2002.

[1] Eddy diffusivity of the surface velocity field in the tropical Pacific Ocean was estimated using satellite-tracked drifting buoys (1979 through mid-1996). The tropical Pacific surface current system is characterized by nonstationarity, strong meridional shear, and an energetic mesoscale velocity field. Eddy diffusivity may be defined as the integral of the autocovariance of Lagrangian eddy velocities, requiring both stationary and homogeneous statistics of the eddy field. Eddy velocities were obtained by removing a splined mean field to eliminate mean shear from observations binned (1) spatially to group data that have similar dispersion characteristics and (2) temporally to create stationary eddy statistics. Zonal diffusivity estimates are up to $\approx$7 times larger than meridional diffusivity estimates in the high eddy energy regions. This anisotropy is associated with the meridional mesoscale wave motion (i.e., by equatorial and tropical instability waves) that increases eddy variance but does not lead to a proportional increase in water parcel diffusion because of the coherent character of the trajectory motion, at least for initial time lags. Simple autoregressive models of first and second order are used to describe and classify the resulting eddy statistics. An independent confirmation of the diffusivity estimate in the central/eastern Pacific was obtained by comparing tracer flux divergence computed from a parameterization using diffusivity estimates of our analysis with that from direct eddy Reynolds stress flux divergence. Our results show that diffusivity can be estimated for regions not considered previously either because of sparse data or the complexities of the velocity field. *INDEX TERMS:* 4568 Oceanography: Physical: Turbulence, diffusion, and mixing processes; 4520 Oceanography: Physical: Eddies and mesoscale processes; 4572 Oceanography: Physical: Upper ocean processes; 4231 Oceanography: General: Equatorial oceanography; *KEYWORDS:* eddy heat flux, horizontal diffusivity, Lagrangian observations, Lagrangian timescale, surface drifters, tropical Pacific

Citation: Bauer, S., M. S. Swenson, and A. Griffa, Eddy mean flow decomposition and eddy diffusivity estimates in the tropical Pacific Ocean: 2. Results, *J. Geophys. Res.*, *107*(C10), 3154, doi:10.1029/2000JC000613, 2002.

1. Introduction

[2] The principal objective of this study is to estimate horizontal eddy diffusivities of the tropical Pacific Ocean surface flow using Lagrangian data (surface drifting buoys). Over the last decade, there has been an emphasis placed on observing the upper tropical Pacific Ocean where the atmosphere is sensitive to anomalous air-sea exchange. The magnitude and distribution of sea surface temperature anomalies (SSTA) are important factors in energy fluxes between the air-sea interface. To obtain improved modeled SSTAs, for example, estimates of horizontal eddy temperature fluxes (ETF) in the upper ocean are required. Horizontal ETF can be computed from parameterizations that relate large-scale horizontal temperature gradients and eddy diffusivity. Herein, we estimate horizontal diffusivities in regions where the complexities of surface currents and sparseness of data have precluded the determination of such estimates until now.

[3] The transport of passive tracers in the ocean depends on the interaction of a broad spectrum of scales of motion

0148-0227/02/2000JC000613

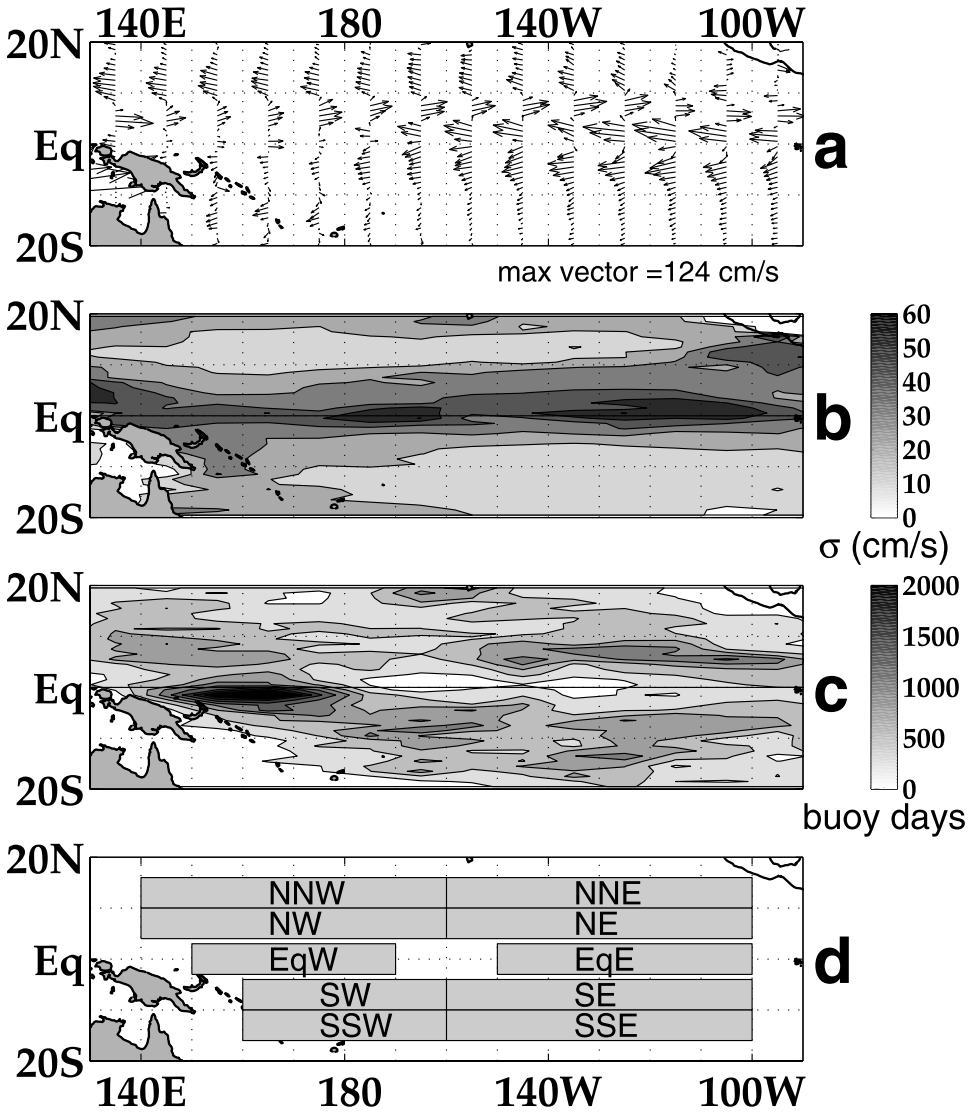

Figure 1. The 1° latitude by 10° longitude surface drifter binned (a) climatological mean velocity, (b) root mean squared (rms) residual velocities, (c) data sampling (in buoy days, <250 buoy days in white), and (d) analysis domain subdivided into regions.

and, therefore, is a complex phenomenon to describe and to predict. Herein, tracer transport is described as a sum of mean (resolved) and eddy (unresolved) motions, for which a spectral gap between the components is assumed. This assumption allows for the decomposition of transport into mean and eddy components, such that eddy velocities, ($\mathbf{u}'$), are computed by the removal of an estimated mean field, ($\mathbf{U}$), from the total Lagrangian velocity estimates, ($\mathbf{u}$). In the context of the advection-diffusion equation, eddy transport is assumed to depend on the spatial derivatives of the large-scale flow. This simple model allows for the parameterization of the unresolved motions via diffusivity estimates when the eddy velocity statistics are homogeneous and stationary, [*Taylor*, 1921].

[4] Surface currents in the tropical Pacific Ocean (Figure 1a) are characterized by strong spatial inhomogeneities (shear in the zonal mean flow characterized by latitudinal bands of large wave activity and varying eddy variance) and strong seasonal variability [*Philander*, 1990; *Frankignoul et al.*, 1996; *Reverdin et al.*, 1994]. Until now inhomogeneity and nonstationarity in the flow have compromised estimates of statistically based eddy transport parameters in these regions of the tropical Pacific. Further, waves and other processes exist that exhibit varying spectral characteristics and may be inconsistent with the assumption of the existence of a spectral gap between mean and eddy components. *Bauer et al.* [1998] (hereinafter referred to as B98) presented a methodology for which the primary goal was to estimate mean flow and diffusivity from Lagrangian data, specifically addressing issues such as spatial and temporal inhomogeneity. To test the method, diffusivity estimates were obtained for two dynamically distinct flow regimes of the tropical Pacific.

[5] The goal of this study is to implement the methodology of B98 to estimate spatial and seasonal horizontal eddy diffusivity for surface currents (10–15 m depth) throughout the tropical Pacific Ocean. Characteristics of the eddy transport statistics are discussed in terms of

statistical models (first- and second-order autoregressive models) and modifications to these models to interpret the eddy transport statistics. Verification, as a part of this analysis, entails computing eddy temperature flux divergence from data in the central and eastern equatorial Pacific, a region known for its complex flows and importance to tropical ocean/atmosphere interactions.

[6] The paper is organized as follows. Basic turbulence statistics theory and the Pacific Ocean surface drifter observations used for the analysis are discussed in section 2. A description of the tropical Pacific surface flow in terms of stationarity and homogeneity is presented in section 3. A subset of data in a relatively simple dynamical regime is analyzed in section 4 for which turbulence statistics are computed to provide a foundation for analyzing more complicated flow patterns. A simple conceptual framework, described in terms of statistical turbulent models, is used to interpret data results (section 5). Seasonal and regional diffusivity estimates are presented in section 6 based on the conceptual framework presented in section 5. Eddy diffusivity estimates of the complex eddy flow of the central/eastern tropical Pacific are used to estimate eddy temperature flux divergence. A comparison with direct estimates derived from Reynolds stress fluxes is presented in section 7. The principal points of the paper are summarized in section 8.

2. Eddy Transport Statistics and Lagrangian Observations of the Tropical Pacific

2.1. Eddy Transport Statistics Using Lagrangian Observations

[7] Lagrangian data are well suited for estimating eddy transport parameters because they provide direct information about the motion of particles in the flow. As noted in B98, the transport of passive tracers depends on the interaction of an infinite number of scales of motion. To develop a more tractable problem, the velocity field is assumed to have two distinct components with scales of motions clearly separated: a mean flow $\mathbf{U}$, characterized by large spatial scales, and a turbulent mesoscale flow $\mathbf{u}'$. This separation of the velocity field into two spectrally distinct components is the basis for the advection-diffusion equation and the parameterization of the eddy activity in terms of eddy diffusivity, κ, [*Taylor*, 1921]. When an eddy field is homogeneous and stationary, κ can be defined as

$$\kappa = \lim_{\tau \to \infty} \kappa^*(\tau); \kappa^*(\tau) = \int_{\tau'=0}^{\tau} R(\tau') d\tau' \qquad (1)$$

where $R(\tau)$ is the Lagrangian autocovariance of a component of the turbulent velocity, $\mathbf{u}'$, computed following the fluid particles. (Examples of generalizations of the definition of diffusivity are discussed by B98, such as *Davis* [1987].) From equation 1, diffusivity is defined only when the asymptotic eddy transport statistics converge: $R(\tau \to \infty) \to 0$; $\kappa^*(\tau \to \infty) \to$ constant. This depends on adequate sampling along with the requirements of homogeneity and stationarity of the eddy velocity field, u'. If homogeneity of the eddy variance is not satisfied, the diffusivity estimate does not accurately represent the diffusivity of the entire region. If stationarity is not satisfied, correlations in $R(\tau)$ will persist with large time lag, τ, which often results in nonconvergent eddy transport statistics and "undefined" eddy diffusivity.

[8] The identification of regions in the tropical Pacific characterized by approximately stationary and homogeneous eddy statistics is discussed in section 3 (see Figure 1d). Note that, even when these regions are identified, it is still possible that the presence of organized motions such as waves or coherent structures might introduce additional complexities in the eddy transport statistics, as discussed in section 5. Also, note that in practical application, an important and delicate issue to address is how to perform the decomposition of the velocity, $\mathbf{u}$, into the two components, $\mathbf{U}$ and $\mathbf{u}'$. This decomposition is the first necessary step in the estimation of the transport components.

[9] The approach commonly used to perform the decomposition consists of estimating the mean velocity as a vector average ($\mathbf{U}_o$) inside prescribed boxes (bins), where $\mathbf{U} = \mathbf{U}_o$ is assumed to be approximately constant. The residual velocity is $\mathbf{u}' = \mathbf{u} - \mathbf{U}_o$. To capture spatial variations in the mean velocity field, especially in regions such as the surface of the tropical Pacific, which is characterized by strong mean shear, small spatial bin size is required. However, due to rapid mean flow advection, drifters do not spend enough time in a bin to estimate diffusivity for which asymptotically long time lags are needed. In contrast, if only coarse resolution of the mean field can be obtained, estimates of particle dispersion in each bin are dominated by mean flow shear rather than by eddy dispersion.

[10] In B98 a different approach is presented, in which the mean field is estimated using an optimized bicubic spline. The problems above are at least partially lessened because a continuous spatially varying mean (rather than a constant mean) is removed: $\mathbf{u}'(\mathbf{x}, t) = \mathbf{u}(\mathbf{x}, t) - \mathbf{U}(\mathbf{x})$. This approach allows removal of particle dispersion that may otherwise have been introduced by mean shear. In B98, estimates of diffusivity computed after removing the spline based mean flow were found to converge even for strongly sheared mean flows within the North Equatorial Countercurrent (NECC) during the height of the tropical instability wave (TIW) season.

[11] In section 3, a first assessment of the mean flow and eddy field structure in the Tropical Pacific is performed using the binning method to compute $\mathbf{U}_o$. This assessment is used primarily to identify regions of approximately homogeneous eddy statistics. In the following sections, a more accurate estimate of $\mathbf{U}(\mathbf{x})$ inside each region is performed using the spline method, and the resulting residual field $\mathbf{u}'$ is used to estimate diffusivity.

2.2. Lagrangian Drifting Buoys and the Tropical Pacific Current System

[12] Eddy diffusivity estimates are computed from Lagrangian drifting buoy data within the surface current domain of the tropical Pacific Ocean. Measurements of near-surface water movements were obtained from satellite-tracked drifting buoys in the tropical Pacific for the Equatorial Pacific Ocean Climate Study (EPOCS) and Tropical Ocean-Global Atmosphere (TOGA) programs during 1979–1996. Sampling and buoy design are discussed in B98, [see also, e.g., *Niiler et al.*, 1995] and a detailed description of the data

sampling and drifting buoy collection are also given, for example, by *Reverdin et al.* [1994].

[13] From the analysis of the drifting buoy data, binned mean velocity estimates (1° latitude by 10° longitude), root mean square (rms) eddy variability, and data density/distribution (buoy days) for the domain of this study are shown in Figures 1a, 1b, and 1c, respectively. Note that the climatological mean current structure (Figure 1a) is a set of zonally coherent currents that are strongly sheared meridionally. The classical tropical surface currents, from north to south, are the westward North Equatorial Current (NEC; north of 10°N), the eastward North Equatorial Countercurrent (NECC; 4°N to 10°N) and the broad westward South Equatorial Current (SEC; south of 4°N). The inhomogeneous nature of the flow field also is reflected in the rms of the residual velocities. These residual velocities (''eddy'' velocities) are derived by removing the binned mean velocities from the full Lagrangian velocity estimates (Figure 1b). Latitudinal bands of high residual velocity variance are noted in regions with strong mean shear such as the climatological NECC and strong SEC flows near the equator characterized by tropical instability wave activity [e.g., *Legeckis*, 1977]. Note that the meridional extent of nearly constant eddy variance is approximately 5° latitude. This is larger than the extent of approximately constant zonal velocities of O(1° latitude). These statistical estimates of climatological quantities are used as guidance for grouping data into regions of similar dynamics resulting in eddy transport statistics representative of the chosen region of interest.

3. Regions of Homogeneity and Stationarity of the Surface Tropical Pacific Eddy Velocity Statistics

[14] Note in Figure 1b, latitudinal bands of approximately uniform RMS eddy velocities are spatially more extensive than the very narrow bands of meridional shear in the zonal velocity field shown in Figure 1a. Therefore, latitudinal bands of constant eddy variance provide logical groupings of data to produce approximately homogeneous eddy statistics. Climatological features, such as a southward shift of the NECC and generally higher off-equatorial eddy variance in the western Pacific, indicate an asymmetry in the statistical nature of eastern and western surface Pacific eddy flow. A longitudinal partition is chosen at 160°W to reflect this east-west asymmetry.

[15] The basic spatial partitioning, chosen according to approximate homogeneity of the rms residual velocities and similar mean flow field within each region, is shown in Figure 1d. For the eastern basin, (160°W to 100°W), the SEC is the prevailing flow in the southern regions (SSE (16°S to 10°S) and SE (10°S to 4°S)) and in region EqE (3°S to 3°N), whereas the eastward flowing NECC is represented in the mean flow of region NE (4°N to 10°N). Region NNE (10°N to 16°N), designated by the predominantly westward flow of the NEC, extends eastward to 110°W rather than 100°W because of coastal flow influences.

[16] The regions west of 160°W are primarily westward extensions of the eastern regions modulated by the seasonal monsoonal effects, the South Pacific Convergence Zone (SPCZ) [region SW (10°S to 4°S) and to some degree SSW (16°S to 10°S)] and other forcing such as westerly wind bursts (WWB's) where the ocean response is predominantly seen in region EqW (3°S to 3°N). Regions SSW and SW extend westward from 160°W to 160°E. The longitudinal extent of these regions is smaller because landmasses and other coastal currents influence the flow west of 160°E. In addition, region SSW observations are sparse west of 170°W. Regions NNW (10°N to 16°N) and NW (4°N to 10°N), primarily influenced by the NEC flow, extend westward from 160°W to 140°E.

[17] In addition to spatial partitioning, temporal partitioning is necessary to ensure statistical stationarity. We ignore interannual variability of the eddy transport statistics due to insufficient sampling in early years of the data set (particularly before 1995). Therefore, temporal partitioning is performed by dividing the data into a climatology of three month groups (Figure 2). This choice is based on several factors. First, a timescale of 3 months is long enough to compute statistically significant estimates over time lags of 25 days. This is important with respect to Lagrangian integral timescales of about 5 days because the asymptotic nature of the Lagrangian statistics can be determined. Second, because seasonal variability in the tropics is usually large, dividing the data into 3 month groupings will determine if these data subsets are stationary. If they are stationary and corresponding diffusivity estimates are defined, this set of temporal groupings will also provide a measure of the seasonal variability in the transport parameter estimates.

[18] Notice that a longitudinal gap in the equatorial band (170°W to 150°W, 3°S to 3°N) is not considered in the analysis (Figure 1d) because sampling density is low (Figure 1c) and flow within this gap appears to be unrelated to that in either EqE or EqW in all seasons. A strong seasonal signal is present in the two equatorial regions, (EqW and EqE), where the dynamics are dominated by equatorially trapped modes associated with rapid oceanic adjustment timescales (e.g., Kelvin waves and Yoshida jets forced by westerly wind bursts (WWBs) confined within the equatorial waveguide [see, e.g., *Bi*, 1995]). Region EqW is unique in the surface current's response to surface wind forcing. Westerly wind bursts in the western equatorial Pacific are atmospheric events that occur primarily from November through February that force surface oceanic eastward flowing Yoshida jets near the equator (Figure 2c). Equatorially convergent flow associated with these events results in meridional oscillations [*Ralph et al.*, 1997].

[19] Other particularly strong seasonal influences are seen in the NECC and equatorial waveguide. In these regions the surface currents weaken dramatically in boreal spring (see Figure 2b), and the NECC may reverse, with the seasonal surface wind forcing [e.g., *Reverdin et al.*, 1994; *Philander*, 1990]. Concurrently, TIW activity is a minimum during this time. In the western basin, the South Equatorial Countercurrent (SECC), the southern hemisphere counterpart to the NECC seen primarily in region SW, occurs during approximately November through February. Note that the most poleward regions, in particular region SSE, are low in eddy energy (Figure 1b) and seasonal variability of the mean flow (Figure 2) [*Reverdin et al.*, 1994; *Bauer*, 2000].

[20] To illustrate the method of computing diffusivity and to show how homogeneity and stationarity are important,

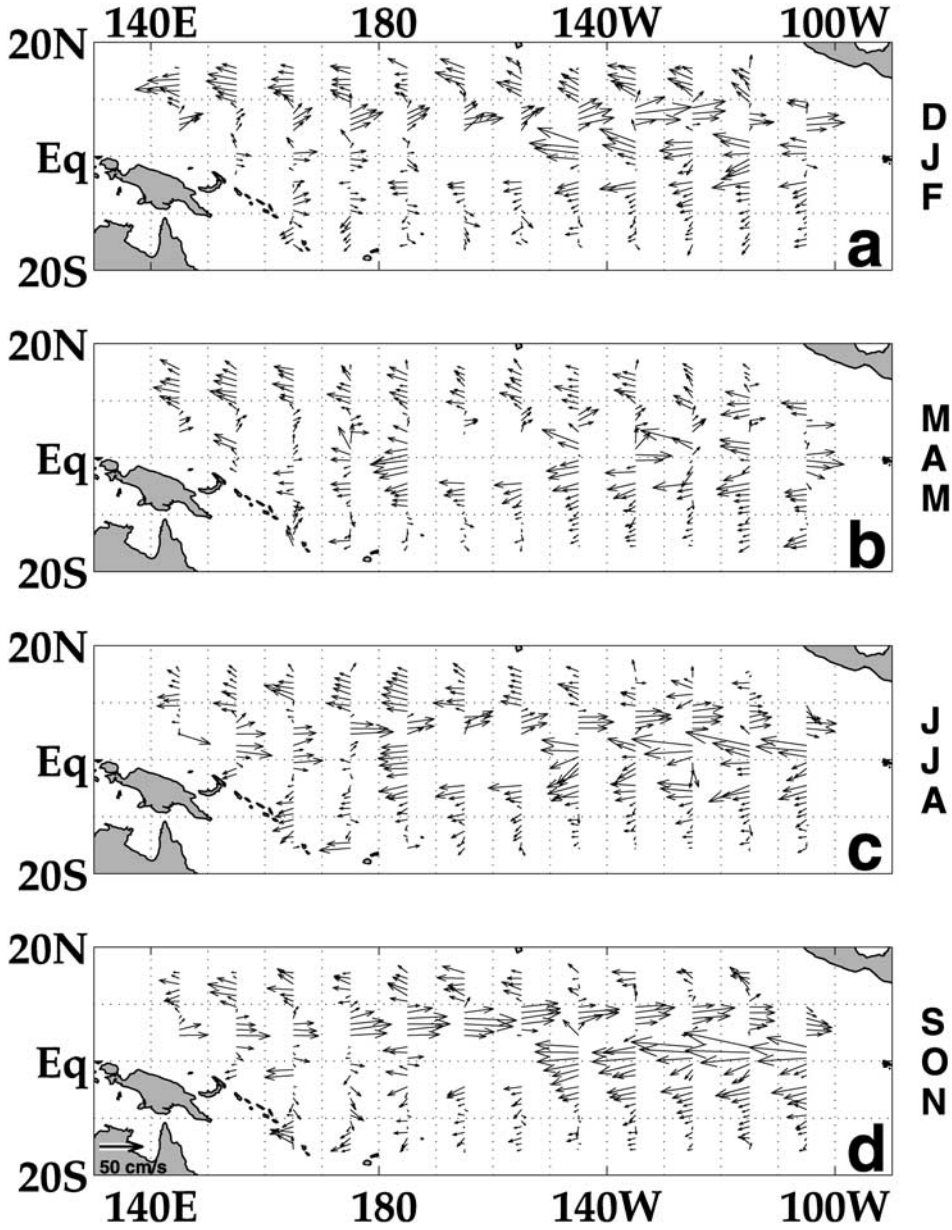

Figure 2. Seasonal mean velocity fields using methodology presented by B98 for (a) December/January/February (DJF), (b) March/April/May (MAM), (c) June/July/August (JJA), and (d) September/October/November (SON) using spline parameter $\rho = 100$ for regions defined in Figure 1d.

we choose to discuss the analysis of the data from region SSE first because of its relatively simple flow characteristics. What follows is a review of the methodology of B98 to highlight difficulties in application that may arise and compromise the requirements of homogeneity and stationarity.

4. Review of Eddy Diffusivity Computation and Example

[21] The flow region SSE (16°S to 10°S, 160°W to 100°W) is characterized by weak and relatively uniform mean velocities (Figure 1a), small eddy variance (Figure 1b) and seasonal variability, (Figure 2) [*Reverdin et al.*, 1994; *Bauer*, 2000], and relatively uniform data distribution (Figure 1c). Since homogeneity and stationarity are basic requirements for the estimation of eddy transport parameters, the data in this region are least problematic for this purpose and highlight advantages as well as possible difficulties in the analysis outlined by B98.

[22] As mentioned in section 2, traditionally eddy velocities have been estimated by partitioning data into regions such that a constant vector describes the mean velocity field throughout a chosen region: $\mathbf{u}' = \mathbf{u} - \mathbf{U}_o$. In this example, the zonal velocity field is examined alone. By estimating a single constant vector mean field, ($\mathbf{U}_o$), any spatial variability of the zonal flow will be lost. When this technique is applied to the full set of data (no temporal binning into seasons or other monthly partitions) of region SSE, the

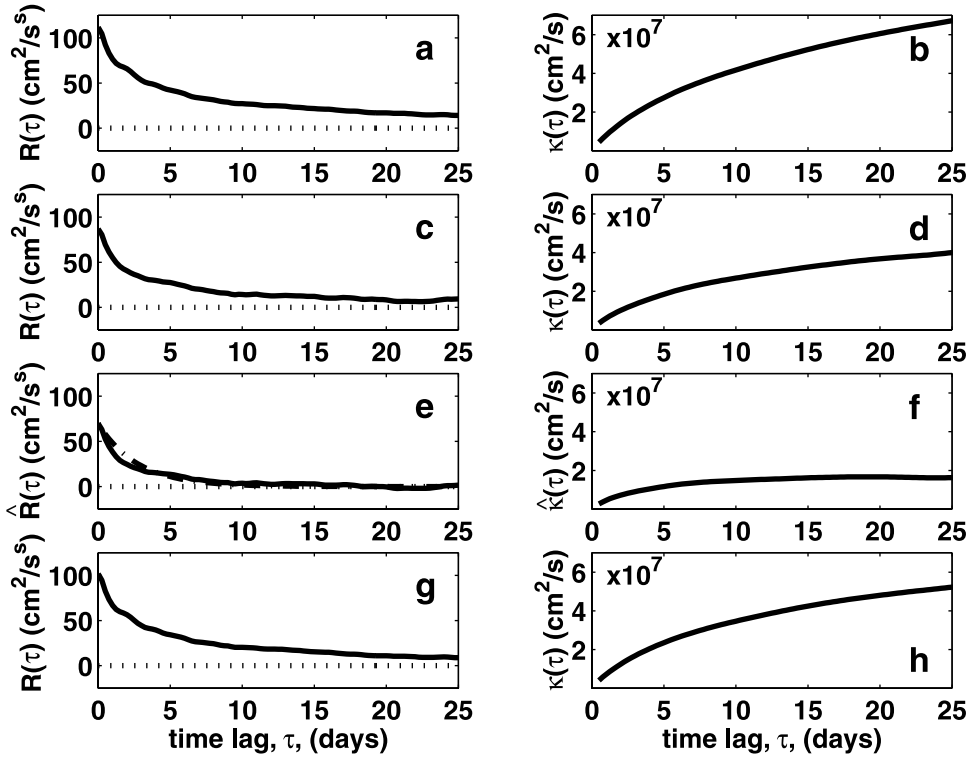

Figure 3. Autocovariance and diffusivity estimates derived from the data of region SSE. (a) Autocovariance estimate using SSE data with no temporal binning and constant vector mean velocity removed; (b) corresponding diffusivity estimate (no temporal binning and constant vector mean removed); (c) autocovariance estimate using SSE data temporally binned (JJA) with constant vector mean removed; (d) corresponding diffusivity estimate (JJA and constant vector mean removed); (e) autocovariance estimate using SSE data with temporal binning (JJA) and spline mean removed and AR(1) process fit (dash-dotted) of exponentially decaying function: $R(\tau) = \sigma^2 \exp(-\tau/T_L)$, $T_L = 2.7$ days; (f) corresponding diffusivity estimate (JJA and spline mean removed); (g) autocovariance estimate using SSE data with no temporal binning and spline mean removed; and (h) corresponding diffusivity estimate using SSE data with no temporal binning and spline mean removed.

zonal autocovariance function does not approach zero within the time scale over which the statistics are computed. Therefore, the integrated autocovariance estimate grows with increasing time lag and the diffusivity estimate is not defined (Figures 3a and 3b). Even if a specific set of months (JJA) is chosen (i.e., temporally binning the data) to obtain approximate stationary flow, the zonal autocovariance estimate still does not approach zero and grows with increasing time lag (Figures 3c and 3d). Therefore, the residual Lagrangian velocity estimates contain the zonal "shear" flow not captured by the constant vector $\mathbf{U}_o$ as well as the eddy flow. The result is a nonconverging estimate of the integrated autocovariance which is a consequence of "shear-enhanced" diffusion rather than the desired eddy diffusion estimate alone.

[23] The description of the mean and seasonal variability of section 3 emphasizes that latitudinal gradients in the mean flow exist throughout much of the tropical Pacific. If a constant vector mean is removed from the full velocity vector, the residual velocity contains both mean flow shear and eddy variability. However, our analysis depends on the residual velocity field representing the eddy component only. B98 describes the use of a least squares, bicubic spline [*Inoue*, 1986] to estimate the mean velocity ($\mathbf{U}(\mathbf{x})$). This approach can minimize the problem of shear contaminated residual velocities because an estimate of the mean velocity field can be determined, ($\mathbf{U}(\mathbf{x})$), for each observation, ($\mathbf{u}(\mathbf{x}, t)$), along the drifter trajectory, ($\mathbf{x}$).

[24] A spline interpolation scheme requires choosing a set of parameters. A thorough discussion of these parameters and the choice of these parameters is presented in B98. The metric, M, introduced in B98, aids in the determination of the optimal values of the roughness parameter, ρ. The metric measures the tendency of the estimated autocovariance $\tilde{R}(\rho)$ to converge to zero and, equivalently, $\tilde{\kappa}^*(\rho)$ to converge to within the limits of sampling errors in the interval bounded by the time associated with the decorrelation of turbulent motions, T_L, and a time that corresponds to $R(T \rightarrow 0)$, $[T_L < t < T]$. This metric (M) is defined as the rms amplitude of the autocovariance function

$$M\left[\tilde{R}(\rho)\right] = \frac{1}{T_{int}} \int_{T_{min}}^{T_{max}} d\tau \left[\frac{1}{\sigma_u^2}\tilde{R}_u^2(\tau;\rho) + \frac{1}{\sigma_v^2}\tilde{R}_v^2(\tau;\rho)\right]^{\frac{1}{2}} \quad (2)$$

and should be minimized over the interval $T_{int} = T_{max} - T_{min}$ such that $T_L < T_{min} < T_{max} < T$. According to the definition, the "best" estimate, for example $\hat{R}(\rho)$ denoted by a carat, is the one that minimizes $M[\tilde{R}(\rho)]$.

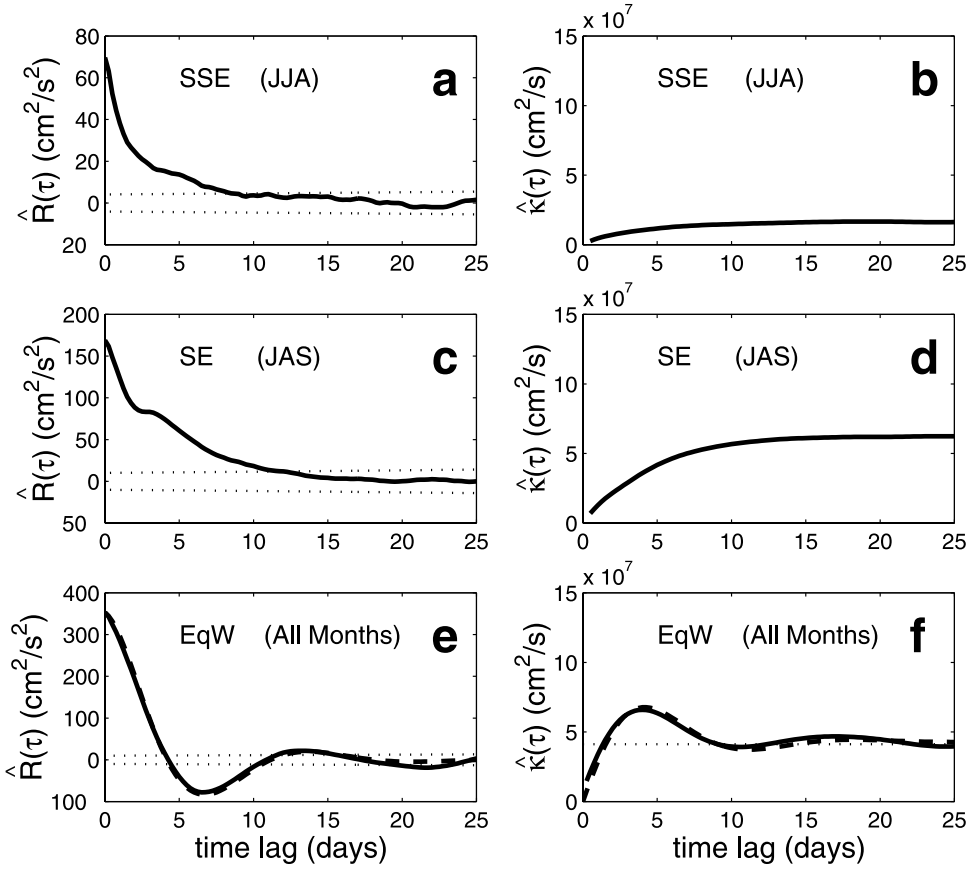

Figure 4. Autocovariance and diffusivity estimates illustrating the various structures of these statistics. Shown are eddy transport statistics obtained from the following regions: SSE (June/July/August (JJA)) zonal (a) autocovariance and (b) diffusivity; SE (July/August/September (JAS)) zonal (c) autocovariance and (d) diffusivity; and EqW (all months) meridional (e) autocovariance and (f) diffusivity. Note that although the diffusivities are scaled the same (Figures 4b, 4d, and 4f), the autocovariances are scaled differently to illustrate the differences in $R(\tau)$ structure.

[25] Conceptually, minimizing M corresponds to minimizing the energy in the fluctuating eddy field at low frequency. From the practical point of view, the value of the optimal ρ is generally chosen to be the smallest ρ along a minimum plateau of the metric so that the resulting mean field is not too noisy. In the present application to the tropical Pacific, it is found that, by choosing $\rho = 100$, even when the minimum roughness along the plateau is less than 100, the errors are typically smaller than the errors in the estimates themselves (see e.g., B98, Figure 3). For simplicity, the value $\rho = 100$ was used throughout our analysis.

[26] When the spatially varying mean flow $\hat{\mathbf{U}}(\rho = 100)$ is removed from the velocity observations of months JJA in region SSE, the zonal autocovariance converges toward zero and the diffusivity reaches an asymptotic value (1.6×10^7 cm^2/s) for time lags less than approximately 10 days (Figures 3e and 3f). Therefore, even for regions with small shear, the removal of a spatially varying mean flow is important to the estimation of these transport parameters. If, instead, there is no temporal partitioning of the data, (although the bicubic splined, spatially varying mean flow, $\hat{\mathbf{U}}(\mathbf{x})$, is removed), a trend remains in the zonal autocovariance function (Figure 3g). The resulting $\tilde{\kappa}_u^*(\tau)$ grows with time lag and eddy diffusivity is undefined (Figure 3h), indicating the importance of temporal partitioning to avoid nonstationary statistics.

5. Conceptual Framework: Basic Turbulence Models and Wave-Modified Turbulence

[27] Before presenting the details of the results of the entire Pacific using the methodology of section 4, we introduce some general concepts that will be useful as a basic framework to interpret the results. In particular, we anticipate that the analysis of the residual field, $\mathbf{u}'$, and of its associated transport in the tropical Pacific, indicates the existence of different turbulent regimes in the various regions. This is exemplified by the different shapes of autocovariances illustrated in Figure 4, corresponding to different space and time partitions.

[28] Shown in Figure 4, the shape of the observed autocovariances varies from an exponential-like shape (Figure 4a), as in the simple case of section 4, to a quasi-exponential shape with a ''knee'' at intermediate lags (Figure 4c), to a wave-like shape (Figure 4e), especially prominent in the meridional autocovariances of near-equatorial regions. While the physical properties of the flow in the various regions and their connection with the turbulence

properties will be discussed in detail in the following sections, a general statistical interpretation of these different properties, in terms of simple stochastic turbulence models, is proposed here. This interpretation will be used as a basis to classify the observed turbulent properties, as well as to compute basic turbulent parameters. Toward this end, a brief overview of the main characteristics of the models and a discussion of their relevance to the observed statistics is presented first.

5.1. First-Order Autoregressive Models and Possible Modifications

[29] The simplest model proposed in the literature [e.g., *Davis*, 1991; *Griffa*, 1996] to describe the turbulent motion of a single particle in an upper ocean eddy field is given by a linear Markov process, or first-order autoregressive (AR(1)) process for the Lagrangian velocity $\mathbf{u}'$ [e.g., *Thomson*, 1987]. For homogeneous and stationary flow, the Lagrangian velocity autocovariance (using the one component only as an example) is given by an exponential,

$$R(\tau) = \sigma^2 \exp(-\tau/T_1), \tag{3}$$

where σ^2 is the variance of $\mathbf{u}'$, and the governing equation is

$$du' = -\frac{1}{T_1}u' + dw \tag{4}$$

where dw is a random increment from a normal distribution with zero mean and variance $2dt \cdot \sigma^2 T_1$. Physically, this means that the particle turbulent velocity has a certain "memory" for timescales on the order of T_1, during which u' tends to "persist". The memory time (T_1) corresponds to the Lagrangian integral timescale (T_L) defined as

$$T_L = \frac{1}{\sigma^2}\int_0^\infty R(\tau)d\tau = \frac{\kappa}{\sigma^2} \tag{5}$$

Using equation 3 in equation 5, it can easily be seen that

$$T_L = T_1. \tag{6}$$

[30] Exponential-like shapes of $R(\tau)$ are commonly found in the literature from the analysis of data from various oceans [e.g., *Figueroa and Olson*, 1989; *Krauss and Bönning*, 1987; *Davis*, 1991]. In the Pacific Ocean, autocovariances like the one in Figure 4a (region SSE) are found in various other regions, suggesting that the simple AR(1) model is in many cases appropriate to describe the underlying turbulent phenomena, at least as a first approximation.

[31] In other regions, a pronounced flattening appears giving rise to a leveling off, or in some cases a secondary maximum (or "knee"), as shown in the example of Figure 4c (region SE). A possible mechanism responsible for the observed "knees" in the autocovariances is associated with the presence of inertial oscillations. If a perfect linear wave is added to a turbulent background, the autocovariance is expected to show a sinusoidal component in addition to the exponential shape. This does not provide a net contribution to diffusivity because particles in perfect wave motion precisely retrace their trajectories in the periodic cycle. However, when the waves are intermittently forced and damped, as are inertial waves, the oscillation may decay quickly after the first cycle, and the wave motion can modify the diffusivity generated by the turbulent background alone. For high frequency waves of relatively low energy with respect to the background turbulence, the waves are expected to act as perturbations to the AR(1) process, giving rise to a "knee" like the one observed in Figure 4c.

[32] Region SE spans latitudes 4°S to 10°S for which the knee shown in the autocovariance of Figure 4c corresponds to theoretical inertial periods ($T_{inertial} = 2\pi/f$) varying from 3 to 7 days, resulting in a broad correlation in $R(\tau)$. Analysis of data from other regions shows similar "knees", consistent with the theoretical dependence of the inertial frequencies on latitude.

5.2. Second-Order Autoregressive Models

[33] AR(1) models with exponential autocovariance (e.g., equations 3 and 4) provide an acceptable framework to describe processes such as those seen in Figures 4a and 4c, where waves can be considered, at most, as perturbations added to a turbulent background. AR(1) models do not appear appropriate, however, for turbulent processes dominated by coherent structures, such as strong vortices or waves. This is the case, for instance, for the wave-like autocovariance of Figure 4e that is characterized by a significant negative lobe. A more appropriate class of models to describe wave-like processes is provided by AR(2) models, where both velocity and acceleration are assumed to be Markov processes [e.g., *Griffa*, 1996; *Berloff and McWilliams*, 2002]. This is the approach that we explore in the following. We mention that a possible alternative to describing processes such as those of Figure 4e is to use AR(1) models "with spin," as recently suggested in the framework of meteorological applications [*Borgas et al.*, 1997; *Reynolds*, 2002]. A comparison between these two approaches will be considered in future work.

[34] The autocovariance that corresponds to an AR(2) process is [*Priestley*, 1981]

$$R(\tau) = \sigma^2 \exp(-\tau/T_2)\cdot\cos(2\pi\tau/T_w + \phi)/\cos(\phi) \tag{7}$$

with a phase relationship, ϕ

$$\sin(\phi) = -\frac{1}{T_2}\cdot\left[\sqrt{\left(\frac{4\pi^2}{T_w^2} + \frac{1}{T_2^2}\right)}\right]^{-1}. \tag{8}$$

This form of the autocovariance is at least qualitatively compatible with the curve obtained from the observational estimate as shown in Figure 4e. Physically, this describes a process where "waves" and "turbulence" cannot be separated. The waves provide the main source of variability in the region, and they are treated as "random" in terms of generation and decay mechanisms.

[35] The waves responsible for autocovariances such as in Figure 4e, are different from the high frequency inertial waves discussed in 5.1, both in terms of frequency and of energy content. As will be discussed in more detail in section 6, these waves can be interpreted as wave motion

in the equatorial band and TIW's, which dominate the variability in the equatorial regions and are characterized by periods of the order 20 days.

[36] The analytical form of the diffusivity can be computed for an AR(2) process using equation 7 according to equation (1):

$$\kappa^{\infty} = \sigma^2 T_2 \left[1 - \left(2\pi \frac{T_2}{T_w}\right)\tan\phi\right] \cdot \left[1 + \left(2\pi \frac{T_2}{T_w}\right)^2\right]^{-1}. \quad (9)$$

[37] In Figure 4f, the shape of $\hat{\kappa}^*(\tau)$ and the asymptotic value of $\hat{\kappa}_v$ are shown for region EqW. It is seen that $\hat{\kappa}^*(\tau)$ reaches a maximum around 5 days and then decreases in correspondence to the integration of the negative lobe of $\hat{R}(\tau)$, stabilizing around a smaller constant $\hat{\kappa}_v$ value at approximately 20 days. The shape of the observed diffusivity (Figure 4f) fits well with the theoretical AR(2) estimate.

[38] Notice that equations 7 and 9 are characterized by two timescales: one which is related to the fluctuation of the dominant wave, with period $2\pi/T_w$, and the other which is related to the equation's envelope of exponential decay, T_2. Neither of these timescales can be interpreted simply as the turbulence memory timescale as for the AR(1) process (equation 3). Moreover, if the integral timescale ($\frac{\kappa^{\infty}}{\sigma^2}$ derived from equation 9) is computed, the resulting timescale is a function of both T_2 and T_w and it does not have an immediate physical meaning as in the case of an AR(1) model.

[39] As will emerge below, the analysis of tropical Pacific drifting buoy data shows that zonal diffusivity estimates are generally modeled approximately as AR(1) statistics, while meridional diffusivity estimates can be modeled as AR(1) or AR(2) statistics depending on the regions. Therefore, a classification of meridional eddy transport statistics in terms of categories A) AR(1) or B) AR(2) models is proposed, and used in the following to describe turbulence transport in the various regions. An important Lagrangian statistic that characterizes the turbulence, i.e., the Lagrangian integral timescale, is interpreted differently for each of the two autoregressive processes. For AR(1) processes, the quantity ($T_L = T_1$) is the exponential decay timescale, a parameter that directly describes the memory of the turbulence. For AR(2) processes, however, κ^{∞}/σ^2 provides a less direct relationship with the characteristic timescales of the diffusive flow. In this case, the decay timescale (T_2) of the envelope may be used as an upper estimate of T_L.

6. Estimates of Eddy Transport Statistics From Drifter Observations

[40] Figure 5 summarizes our zonal and meridional eddy diffusivity estimates for the entire tropical Pacific derived from drifter data over the time interval 1979–1996 using the space-time partitions described in section 3. Notice that in some of the space-time regions, estimates are undefined and they are indicated as extracted blank sections in Figure 5. They correspond to regions of particularly poor sampling or of especially high nonstationarity, where the diffusivity $\kappa^*(\tau)$ is not found to asymptote within the estimate of 3–5 T_L.

[41] The results of Figure 5a suggest that there are regions of maximum zonal diffusivity localized in the equatorial waveguide and in regions of the NECC, where the eddy variance is largest. In contrast, meridional diffusivity estimates are consistently smaller everywhere across the tropical Pacific (Figure 5b). The reasons for this anisotropy will be analyzed in detail in sections 6.2.1–6.2.2. The significance of the results will be discussed, and it will be shown that the difference between zonal and meridional diffusivity is primarily related to a difference in the autocovariance structure (reflecting a difference in the turbulent properties), rather than to a difference in turbulent mesoscale variance. In particular, the meridional mesoscale motions appear dominated by wave activity, i.e., by equatorial waves and TIWs. Wave motion increases eddy variance, but it does not lead to a proportional increase in water parcel diffusion. This is because wave motion is coherent at initial times, so that particles undergo substantial initial displacements but are then returned by the wave, therefore the actual dispersion is much lower than what is suggested by the initial displacement. In other words, wave activity produces meridional autocovariance functions that more closely resemble an AR(2) model with a large negative lobe. Hence, the meridional diffusivity ($\kappa^*(\tau)$), which corresponds to the integral of the autocovariance, does not increase proportionally with eddy energy. This point will be revisited in sections 6.2.1–6.2.2.

[42] Further analysis is aided by classifying regions, according to their meridional eddy transport statistics, into two basic statistical models: AR(1) and AR(2). Regions where meridional eddy flow is modeled approximately by AR(2) statistics are characterized by the strong shear flows of the NECC/SEC, high eddy energy and TIW activity and strong seasonal variability (see section 3). These regions are NE, EqE and EqW, (Figures 1a and 1b). In contrast, regions whose zonal and meridional eddy transport statistics are characterized by an AR(1) model generally exhibit much lower mean current shear and eddy variance with only moderate seasonal variability. The latter are located farther from the equatorial waveguide where there are no strong lateral mean shear flows. They correspond to regions NW, NNW, NNE, SW, SE, SSW, and SSE (Figure 1). This study now considers Category A eddy transport statistics modeled approximately as an AR(1) process and Category B, as an AR(2) process.

6.1. Category A (Off-Equatorial SEC and NEC Flow)

[43] Eddy flow in the westward currents poleward of 4° latitude exhibit zonal and meridional eddy transport statistics that can be approximately modeled by an AR(1) process, but are modified by inertial wave oscillations as described in section 5.1. Since regions span several latitudes, the inertial waves exhibit oscillations of local minima/maxima in the estimated autocovariance functions by virtue of the theoretical latitude-dependent band of inertial wave periods. The eddy transport statistics of data from June/July/August (JJA) of region SSE (Figures 4a and 4b) is an example of the nearly AR(1) nature of Category A eddy flows. In almost all non-equatorial regions, a slight anisotropy exists such that zonal diffusivity estimates are larger than meridional eddy diffusivity estimates (Figures 5a and 5b).

[44] Regions of Category A include those poleward of 10° latitude (SSE, SSW, NNE, and NNW) and most of those between 4° and 10° latitude (NW, SE, and generally SW).

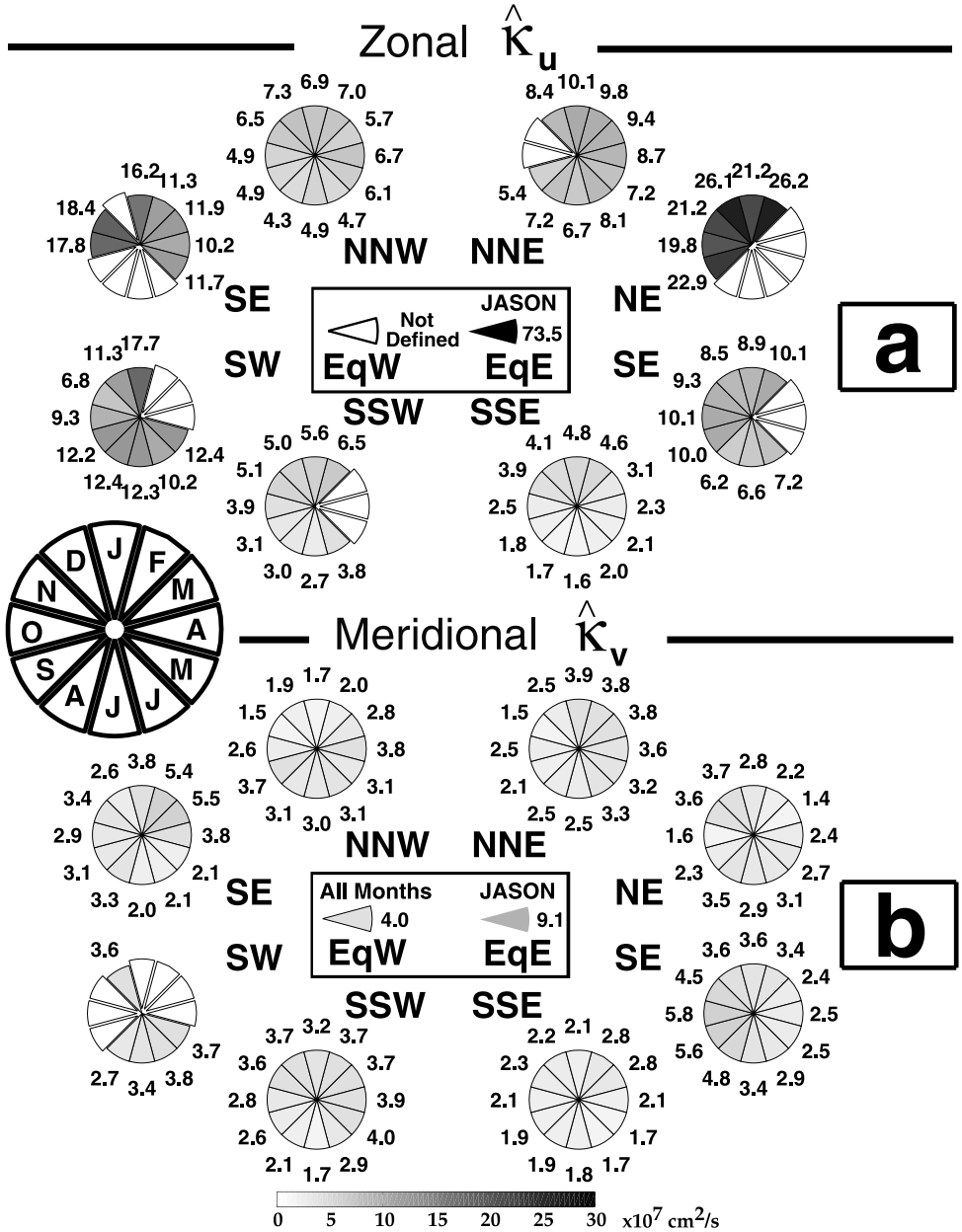

Figure 5. Summary of (a) zonal and (b) meridional diffusivity estimates from analysis. Diffusivity is computed for 3 month partitions centered on the month given in the large circle at left (e.g., J = = December/January/February) except for the equatorial regions (estimates of region EqE uses 5 months (JASON) and no zonal estimates for region EqW are defined while all 12 months are used in the meridional EqW diffusivity estimate). Diffusivity values are indicated in encircling pies in units of $\times 10^{-7}$ cm^2/s and by the color bar at the bottom. Extracted sections refer to subsets of data for which diffusivity estimates are undefined (no number indicated).

Their zonal diffusivity estimates are commonly less than 15 $\times$ 10^7 cm^2/s and meridional diffusivity estimates do not exceed 6 $\times$ 10^7 cm^2/s. Diffusivity estimates are usually lowest in the most poleward regions where mean flow shear and seasonal variability are low.

[45] The seasonal variability in the eddy transport statistics of regions SSE, NNW and NNE follow a similar pattern for which late and early calendar months are characterized by maximum zonal diffusivity. Eddy transport statistics from region SSE can serve as a representative example for most poleward regions. Inertial wave activity is a minimum during months JAS (Figure 4a). Eddy variance associated with inertial wave activity increases in the latter half of the year and both diffusivity estimates and $\hat{T}_1$ increase. Here, intermittently forced inertial waves may enhance eddy transport as indicated by the zonal and meridional diffusivity estimates of region SSE (Figure 5) [*Bauer*, 2000]. Although seasonal eddy transport statistics of NNW and NNE are similar to those of region SSE, there are some differences. For example, diffusivity estimates in region

NNE are slightly larger with slightly less seasonal variability. Zonal variance, in particular, tends to be larger resulting in larger $\hat{\kappa}_u$, and is consistent with other observational analyses [e.g., *Stammer*, 1997], although some estimates are not reported (SON through NDJ) due to poor sampling.

[46] Eddy transport statistics of region SSW are similar to those of other regions poleward of 10° latitude except during the months February through May. During this time, the South Equatorial Countercurrent (SECC) develops and decays and may contribute to nonstationary, nonconvergent eddy transport statistics (Figure 5a). Similarly, zonal diffusivity estimates are not defined either during this time frame in region SW. However, between 4°S and 10°S, zonal diffusivity estimates are larger than more poleward regions, perhaps because of the climatologically stronger mean flow shear and subsequent increased turbulent diffusion closer to the equator. In region SE, strengthening mean flow shear may be responsible for nonstationary eddy transport statistics during FMA through AMJ in contrast to the variability of the SECC in region SW. Region NW, however, is characterized by nonstationary eddy transport statistics during the boreal summer months that may be associated with summer monsoonal activity.

6.2. Category B (Equatorial Waveguide and NECC Flow)

[47] Regions of Category B are located in the strong mean flow of the NECC and SEC (in particular regions NE, EqE and EqW of Figure 1d). In these latitude bands, the highest eddy variance of the tropical Pacific is observed for which a large fraction of the eddy variance is attributed to wave activity (e.g., TIWs). Another feature common to these regions is strong seasonal variability in the mean velocity field and seasonal variability in the eddy variance as well, [*Reverdin et al.*, 1994; *Bauer*, 2000].

[48] The eddy transport statistics from the regions of Category B are distinct from those in Category A. Zonal diffusivity estimates (see Figure 5a) tend to be significantly larger (approximately 20 to 70 $\times$ 10^7 cm^2/s) than those from other regions even though they are similarly modeled by AR(1) statistics. In contrast, meridional diffusivity estimates (Figure 5b) are similar in magnitude to the estimates of other lower eddy energy regions but modeled more appropriately by AR(2) statistics. This is the principal discriminating characteristic between Category B and Category A eddy transport statistics, where $\hat{R}_v(\tau)$ is dominated by a large negative lobe that is associated with large meridional excursions (e.g., Figure 4e). In the central and eastern Pacific, TIWs are well-documented features that contribute to both the high eddy energy and the high correlations in the meridional autocovariance function. Another prominent source of meridional correlations in $\hat{R}_v(\tau)$ is seen in response to forcing by WWBs in the western equatorial Pacific [e.g., *Ralph et al.*, 1997]. Some of these events are heavily sampled and may bias the statistics toward specific events.

[49] Although seasonal variability is considered for Category A flows, seasonal variations introduce nonstationarity in Category B eddy flows to such an extreme that the estimation of eddy diffusivity is compromised in many 3 month periods of the seasonal cycle (white pie wedges in Figure 5). The general features of the eddy transport statistics of Category B regions (NE, EqE, EqW) permit a rough classification based on the AR(2) models of the meridional eddy transport statistics. However, there are differences in the central and western Pacific waveguide and the central and eastern Pacific NECC regions. These three regions are discussed in sections 6.2.1–6.2.3.

6.2.1. Region NE (4°N to 10°N, 160°W to 100°W)

[50] Located in the NECC flow, between 4°N and 10°N in the central and eastern Pacific, region NE captures Lagrangian flow that is influenced by strong mean meridional shear and eddy variance during the season of high TIW activity (boreal late summer, fall and winter). Examples of autocovariances and diffusivities for the zonal and meridional components are shown in Figures 6a and 7a, respectively, obtained for the period DJF, characterized by strong TIW activity. It can be seen that both zonal and meridional eddy transport statistics show signatures of inertial waves, corresponding to approximately 3–7 day periods. As mentioned above, in this region, zonal diffusivity (approximately modelled as an AR(1) process) is much higher than meridional diffusivity (approximately modelled as an AR(2) process). For example, for DJF, the zonal diffusivity is $\hat{\kappa}_u \approx 21 \times 10^7$ cm^2/s (Figure 6a), while the meridional diffusivity is $\hat{\kappa}_v \approx 2.8 \times 10^7$ cm^2/s (Figure 7a). The nature of this anisotropy is discussed in detail in the following.

[51] As a first step, the significance of the observed anisotropy is investigated. Since the large scale mean flow is strongly anisotropic and sheared in this area, it is important to verify that the decomposition is done correctly and that the zonal statistics are not contaminated by residual large scale correlations. Qualitative evidence supporting the validity of the estimates is provided by the values of the zonal and meridional variances (Figures 6a–7a), which are very similar, $\sigma_u^2 \approx \sigma_v^2 \approx 500$ cm^2/s. This indicates that both components of the residual fluctuations are equally energetic, and suggests an accurate representation of the mean and a correct removal of this mean. To quantitatively support the validity of the estimates, the structure of the zonal autocovariance $\hat{R}_u(\tau)$ and diffusivity $\hat{\kappa}_u^*(\tau)$ (Figure 6) can be considered. As discussed in section 4 and as shown in details in B98, when the mean shear is not correctly removed, it leads to a residual correlation in $R(\tau)$, preventing the asymptotic behavior $R(\tau \rightarrow \infty) \rightarrow 0$, $\kappa^*(\tau \rightarrow \infty) \rightarrow$ constant. The autocovariance $\hat{R}_u(\tau)$ in Figure 6a approaches zero (at least within the error limits) at time lags τ less than 20 days, while $\hat{\kappa}_u(\tau)$ approaches a constant. This behavior strongly suggests that the mean shear is correctly removed and that the energy of the fluctuation is correctly minimized at low frequencies. Note that, if the details of the autocovariance function are compared to the ideal AR(1) exponential behavior, $\hat{R}_u(\tau)$ shows some residual correlation at the intermediate lags of 15–25 days. This residual correlation could indeed come from unresolved shear, but it would account for only ≈20% of the diffusivity value, which lies inside the error level (see B98, Figure 3a). Since the zonal diffusivity estimates for region NE are almost one order of magnitude larger than the meridional estimates, and this residual correlation effect cannot explain this discrepancy, there is compelling evidence that the anisotropy is significant.

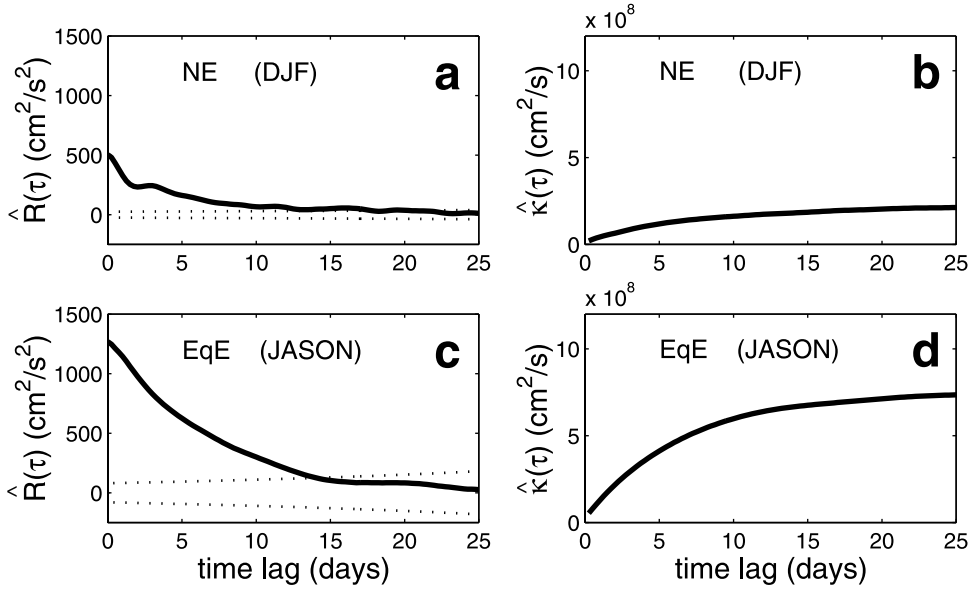

Figure 6. Zonal eddy transport statistics for region NE (DJF) (a) autocovariance and (b) diffusivity and region EqE (JASON) (c) autocovariance and (d) diffusivity. Dotted lines are estimates of the 95% confidence intervals around zero for the autocovariances computed as $\pm 2(1/n_L^*)^{1/2}$, where n_L^* is the number of independent measurements for each time lag [*Priestley*, 1981].

[52] As a second step, we investigate the nature of the different shapes of the zonal and meridional autocovariances (Figures 6a–7a). This difference is responsible for the different values of the diffusivities κ_u and κ_v, since the variance values are approximately the same. In particular, the fast decay and the negative lobe in the meridional autocovariance are responsible for the low values of κ_v. Conceptually, the reasons for the different zonal and meridional autocovariance estimates $R(\tau)$ are not immediately obvious, since it might be expected that particles in a TIW disturbance should exhibit symmetric oscillations in the zonal and meridional directions. On the other hand, as shown by *Flament et al.* [1996] for a specific event during November and December 1990, trajectories tend instead to be cycloidal. In other words, they are characterized by a superposition of rotation and westward translation, with a drift that can vary significantly in different realizations. For example, the translation speed may vary as much as 50 cm/s (between 30 cm/s and 80 cm/s). On the basis of these observations, and a number of others including ADCPs, satellite, and hydrographic measurements, *Flament et al.* [1996] suggest that TIWs should be interpreted as "finite amplitude disturbances drifting along the shear layer between the SEC and the NECC", rather than as purely linear waves. This can have important implications from the transport point of view. Kinematically, the trajectories show an almost cusp-like structure, with the meridional component oscillating between different latitudes, while the zonal component is mostly influenced by advection bursts (suppressions) at latitudes where the westward drift is in the same (opposite) direction as the mean shear. Consequently, the eddy transport in the meridional direction is dominated by damped wave processes and its statistics are described by an AR(2) model, whereas the transport in the zonal direction is dominated by advection fluctuations without significant oscillations and its statistics are described by an AR(1) model.

[53] The zonal eddy transport statistics for DJF (Figure 6a) suggest values of $\hat{\kappa}_u \approx 21 \times 10^7$ cm^2/s and $\hat{T}_1 = \hat{T}_L \approx 4$ days, (see equations 5 and 6 for the mathematical relationships of the turbulent parameters for an AR(1) process). The range of $\hat{\kappa}_u$ values for all the 3 month partitions (Figure 5a) is approximately $19-24 \times 10^7$ cm^2/s. The meridional diffusivity estimates, $\hat{\kappa}_v^*(\tau = 25\text{d})$, instead, fall between 2 and 4×10^7 cm^2/s for each 3 month grouping (Figure 5b). These consistently low values of $\hat{\kappa}_v$ supports the idea that the large eddy variance associated with TIW activity does not contribute greatly to meridional diffusivity. That is, when the eddy energy increases with increased TIW activity through the seasonal cycle, the meridional diffusivity does not increase, in contrast to AR(1) model results (equations 5 and 6). A simple AR(2) fit to the meridional autocovariance function for DJF (Figure 7a) and its integrated form show a qualitative agreement, even though deviations from the AR(2) model, possibly due to intertial wave correlations, can be noticed. In particular, the fit does not provide an adequate estimate of diffusivity because it attempts to force a solution using the variance ($\hat{R}(\tau = 0)$), the time lag of the first zero crossing and, the time lag and maximum value of the negative lobe. Inertial wave correlations cause a deviation from the decay modeled by an AR(2) process and therefore are a prominent source of the departures noted in the observed $\hat{R}_v(\tau)$ (Figure 7a).

[54] As a final remark, we note that even though the anisotropy between zonal and meridional components appears significant and well motivated from the physical point of view, it is important to keep in mind that there are several technical points in the present analysis which might influence the details of the results. For instance, it should be considered that TIWs, even though they might be randomly located over tens of degrees of longitude, are confined within a narrow latitude band in the zonal direction. As a consequence, when a zonal mean is performed, the meri-

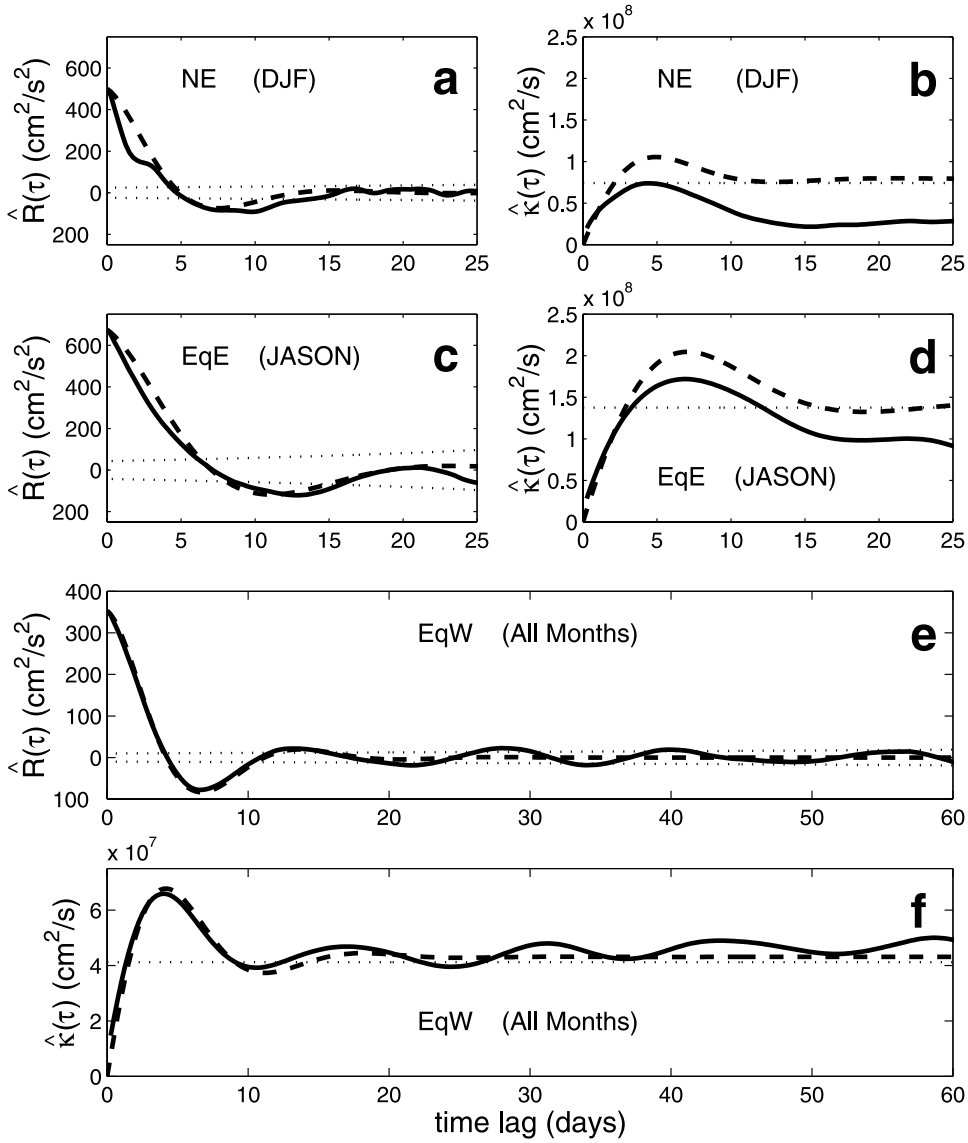

Figure 7. Autocovariance and diffusivity estimates of AR(2) meridional eddy velocity flow. Region NE (DJF) (a) autocovariance and (b) diffusivity; region EqE (JASON) (c) autocovariance and (d) diffusivity; and region EqW (all months) (e) autocovariance and (f) diffusivity. Solid curves represent estimates from spline-removed residual observations. Dashed curves represent AR(2) fits to the observational estimates. Dotted lines in autocovariance estimates (Figures 7a, 7c, and 7e) are estimates of the 95% confidence intervals around zero computed as $\pm 2(1/n_L^*)^{1/2}$, where n_L^* is the number of independent measurements for each time lag [*Priestley*, 1981]. Dotted lines in diffusivity estimates (Figures 7b, 7d, and 7f) represent the asymptotic value of the analytical fit of the integrated autocovariance, κ_ν^∞ (see equation 9).

dional flow associated with TIWs nearly cancel and the TIW contribution mostly remains in the residual/eddy component. The zonal TIW flow, instead, being more localized, might be estimated as part of the mean. Also, the results could at least be partially sensitive to the details of the specific choice of partition (Figure 1c). The present choice of latitudes bordering regions NE and EqE separates the latitudes of eastward TIW flow in the northern (NE) latitudes and the westward TIW recirculation in the southern (EqE) latitudes. Since this partitioning does not capture all of the TIW flow into one region, "reconstructed" trajectories of fluid parcels from residual velocities might not be retraced. On the other hand, a different partition that includes both NE and EqE in a single region does not appear feasible from the point of view of homogeneity requirements. Equatorial dynamics, in fact, are significantly different and the values of eddy variance (eddy kinetic energy) (Figure 2b) vary between NE and EqE so that homogeneity of the eddy statistics is not met if the two regions are merged.

[55] Finally, we notice that the interannual variability might also play a role in "masking" the zonal component of TIWs. The data used in this study represent a climatology. Therefore, the zonal mean flow field will not reproduce

the translational velocity for any specific TIW season and oscillations in the zonal eddy transport statistics might be reduced.

6.2.2. Region EqE (3°S–3°N, 160°–100°W)

[56] Region EqE is located in the northern part of the SEC, that straddles the equator, where eddy variance is large and seasonal variability of the mean and eddy variance is also large. Adding to the complexity of the flow in region EqE is the complex nature of equatorial waveguide dynamics. Here meridional Ekman transport induces divergence within a few degrees of the equator. This results in the poleward advection of surface drifters with the added consequence of low sampling because of drifter residence times. The seasonal cycle produces a strong mean flow and results in large TIW activity. The TIW activity in region EqE is similar to that seen in region NE except that the southern branch of TIW circulations are included in this region rather than the eastward flow of the northern branch which is captured in region NE.

[57] Because the response time is rapid in the equatorial waveguide, and sampling is limited due to mean meridional Ekman divergence, 3 month temporal bins result in inadequate sampling. From late boreal summer through fall and winter, the surface current system is well established and nearly stationary. Hence, a 5 month data subset beginning in July and extending through November (JASON) is used to improve the sampling. Other 3 month periods, particularly during the relaxation of the NECC from March through May, preclude the estimation of eddy diffusivity.

[58] Similar to the results of region NE, the zonal eddy transport statistics of region EqE are approximately modeled by an AR(1) process (Figure 6b). However region EqE is distinguished from region NE in the magnitude of zonal variance ($\approx$1200 cm^2/s), which is approximately double the meridional estimate. Also, the diffusivity $(\hat{\kappa}_u)$ is about 3 times larger (73.5×10^7 cm^2/s) than that computed for 3 month partitions in region NE. This large value of zonal eddy diffusivity may reflect complex dynamical processes such as equatorial wave responses, rapid mean flow adjustment, and sampling issues. Another distinguishing factor relates to the absence of inertial oscillation correlations in the eddy transport statistics because Coriolis effects are less important near the equator (the inertial wave period at 3° latitude is greater than 10 days and increases rapidly toward the equator).

[59] Meridional eddy transport statistics estimates for JASON are shown in Figures 7c and 7d. Here, inertial oscillations are absent and the agreement between estimated $\hat{R}_v(\tau)$ and $\hat{\kappa}_v^*(\tau)$ are more similar to an AR(2) process than the estimates computed for region NE. For the region EqE meridional estimates, an AR(2) model fit provides an estimate of the envelope of decay time: $\hat{T}_2 \approx 6.8$ days.

6.2.3. Region EqW (3°S–3°N, 150°E–170°W)

[60] Region EqW is the western counterpart of region EqE. The currents in region EqW are different from the climatological patterns of mean flow in the central and eastern Equatorial Pacific because the NECC is shifted southward into this latitudinal band near the Equator and west of the dateline. West of the dateline, the maximum eddy variance and its seasonal variability are restricted to a narrow equatorial band (see B98, Figure 1b). In contrast to the poor sampling in the central and eastern equatorial Pacific, sampling density is a maximum in region EqW (Figure 1d). This is due in part to the differences in meridional Ekman dynamics. It is also a consequence of concentrated deployments related to studies of oceanic responses of WWB's, [e.g., *Ralph et al.*, 1997; *Bi*, 1995]. Therefore, any analysis of this region's data will be biased toward these events and may not represent a climatological manifestation of the eddy transport statistics.

[61] Noting that this inherent bias of the sampling exists, $\hat{R}_v(\tau)$ and $\hat{\kappa}_v^*(\tau)$ shown in Figures 7e and 7f are similar to those of regions NE and EqE. Here, the data partitioning may play a role in zonal eddy transport statistics that are similar to those of the AR(1) model. Similar waveguide dynamics are expected in both EqW and EqE regions. However, due to rapid response time of the surface velocity field, estimates of zonal eddy transport statistics are not stationary for each of the 3 month data subsets. A typical example of the rapid response time is acceleration and deceleration of order weeks to a month of eastward flowing Yoshida jets during the late and early months of the year in response to WWB forcing. Because of the nature of this zonal nonstationary eastward surface flow, diffusivity estimates are not computed for this region.

[62] Although eddy variance is large, the meridional diffusivity $(\hat{\kappa}_v)$ is similar in magnitude to other meridional estimates elsewhere in the tropical Pacific domain. A similar result is seen in the eddy transport statistics for regions EqE and NE. Therefore, the meridional eddy transport statistics can be approximated by AR(2) statistics and are a consequence of large magnitude wave oscillations that suggest the existence of TIW's. Confirming their existence however, is difficult. Upwelling in the shallow mixed layers of the central and eastern equatorial Pacific creates a substantial meridional SST gradient that can be used as an indicator of surface flow variability (spatial and temporal). This meridional gradient is absent in the western equatorial Pacific where the deep warm pool exists and Ekman divergence patterns differ from those of the central and eastern Pacific. TIW events are denoted prominently by trains of cusped, wave-like patterns in satellite imagery in upwelling regions [e.g., *Legeckis*, 1977], but small meridional SST gradients in the EqW region compromise the detection of these TIW events.

[63] The large eddy variance and the meridional eddy transport statistics indicate wave-like features are present in region EqW. The timescale of these oscillating features is comparable to, or somewhat shorter (10–15 days), than those seen in the eddy transport statistics of region EqE (greater than 20 days). During the TIW season (beginning in June and lasting until December/January/February), oscillations in the meridional autocovariance function ($\hat{R}_v(\tau)$) generally damp out rapidly, which is similar to the eddy transport statistics of regions EqE and NE. During the boreal spring months, when TIW activity is mostly absent in regions NE and EqE, oscillations in $\hat{R}_v(\tau)$ persist through time lags of 30 days of time lags. These correlations in $\hat{R}_v(\tau)$ may be associated with the large meridional excursions experienced by surface drifters described by *Ralph et al.* [1997]. Conceptually, WWB's set up an eastward Yoshida jet in the equatorial waveguide that causes convergence toward the equator and an overshooting "oscillation" with periods of approximately 10 to 15 days, [*Ralph et al.*, 1997].

These events are well sampled (Swenson and Olson, personal communication) and may therefore bias the estimates of meridional eddy transport statistics. Although both TIW and WWB activity overlap seasonally, waves of similar variability and timescales are found in all of our 3 month data subsets suggesting that a combination of TIW activity (July through December) and WWB-activated meridional oscillations may be taking place (coincidentally or in separate seasons).

[64] Eddy transport statistics of EqW observations using all data (no temporal partitioning) show small amplitude correlations out to a time lag of 60 days (Figures 7e and 7f). An AR(2) model of the autocovariance ($R(\tau)$) and diffusivity ($\kappa^*(\tau)$) is designated by a dotted line. In this case, the decay and first negative lobe result in a diffusivity of 4.0×10^7 cm^2/s with $\hat{\kappa}_v^{\infty} = 4.1 \times 10^7$ cm^2/s. The decay envelope timescale is $T_2 \approx 4.8$ d, and is similar in magnitude to that in region NE.

6.3. Lagrangian Integral Timescales

[65] The analysis of turbulence statistics obtained from Lagrangian observations in Category A regions indicates that zonal estimates of autocovariance ($R(\tau)$) and diffusivity ($\kappa^*(\tau)$) are closely approximated by a linear Markov (AR(1)) process with minor deviations due to inertial oscillations. The meridional statistics also approximate an AR(1) process with exponentially decaying $R(\tau)$ where wave features (e.g., TIWs) do not dominate the variability of the residual velocity estimates. Where wave features do exist (Category B regions consisting of the equatorial regions and region NE), the autocovariance function deviates from, but is similar to an AR(2) process (see discussion in section 6.2).

[66] The Lagrangian timescale for an AR(1) process can be interpreted in terms of a statistical turbulence model where $T_L = T_1$ is the e-folding scale or intrinsic (decay) timescale of the autocovariance ($R(\tau)$). For an AR(2) process, T_L is a function of two timescales and does not have a direct interpretation as the intrinsic scale of the turbulence. *Rossby et al.* [1983] and *Swenson and Hansen* [1999] suggest that the turbulent timescale (T_L) is approximately a "regional" constant, so that the diffusivity, (κ), is scaled by the residual velocity variance, σ^2 (equation 5). This hypothesis is tested by plotting $\hat{\kappa}$ versus $\hat{\sigma}^2$ estimates from all the data in the various regions except the zonal estimates in regions EqE and EqW. The results for both zonal and meridional components are shown in Figure 8. Here, the zonal estimates approximately fit a straight line (least squares linear fit) with $\hat{T}_L^u = 5.48 \pm 1.30$ days (denoted by open circles) and correlation coefficient, $r^2 = 0.96$.

[67] Some of the meridional estimates (denoted by crosses) are distributed quite differently from the zonal estimates. For region NE, diffusivity is essentially independent of eddy energy $(\hat{T}_L^v)_{NE} = 0.25 \pm 0.22$ days and correlation coefficient, $r^2 = 0.45$. This indicates that T_L is not a representative decay timescale of the eddy flow. In fact the timescale, (T_L), in the presence of waves (AR(2) process) does not correspond to the intrinsic scale for an AR(1) process, but it is expected to be smaller because of the integration of the negative lobe in the autocovariance, $R(\tau)$, (see equations 7 and 9 in section 5.2). Any parameterization describing the residual velocity field in the TIW regions should be modeled differently from the AR(1) processes of other regions. As suggested above, the timescale of the AR(2) process, T_2, may be used as an upper bound on T_L since the exponential decay envelope is associated with the turbulence decorrelation and with the magnitude of the negative lobe in the autocovariance ($\hat{R}_v(\tau)$).

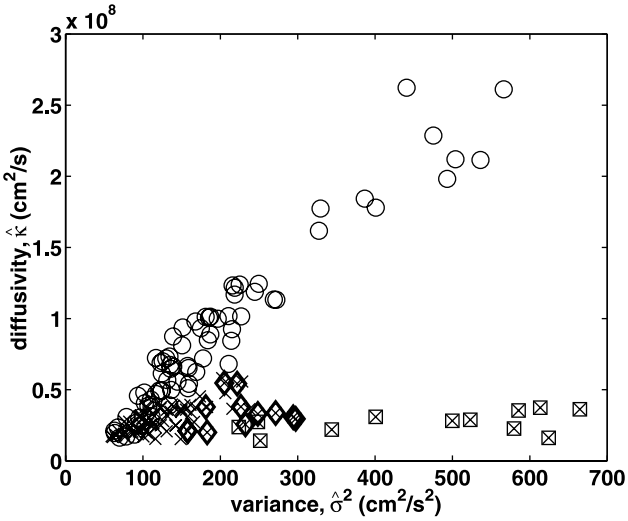

Figure 8. Estimates of diffusivity versus variance: $T_L = \frac{\kappa}{\sigma^2}$. Open circles represent zonal estimates; crosses denote meridional estimates. Crosses enclosed within squares are meridional estimates of the data in region NE, and crosses enclosed within diamonds are meridional estimates of data in region NW.

[68] Although the functional form of the Lagrangian integral timescale (T_L) depends on the statistical models AR(1) or AR(2) that represent the eddy flow, the diffusivity (κ) always provides a direct estimate of turbulent diffusion (if homogeneity and stationarity conditions are met) regardless of wave activity. To assess whether or not the magnitudes of the computed diffusivity estimates are reasonable, comparisons were made between parameterizations of tracer flux divergences and direct eddy Reynolds flux divergences. This analysis follows.

7. Eddy Temperature Flux Divergence

[69] The redistribution of heat by the eddy velocity field plays a critical part in the estimation and prediction of global climate variability. It is important, therefore, to estimate the divergence of temperature by the eddy motions. Direct measurements of eddy temperature flux divergence (ETFD) are possible because the surface drifters not only record distances traveled (providing velocity estimates) but also measure the mixed layer temperature. A comparison is now made between a flux gradient model that employs an eddy diffusivity parameterization with those derived from direct measurements of ETFD using Reynolds stress statistics ($\langle v'T' \rangle$).

[70] Herein, our focus is on the central/eastern Pacific Ocean meridional ETFD. This is a very active region (high eddy variance associated with TIW activity) where large meridional eddy temperature flux divergences have been computed [*Hansen and Paul*, 1984] (hereinafter

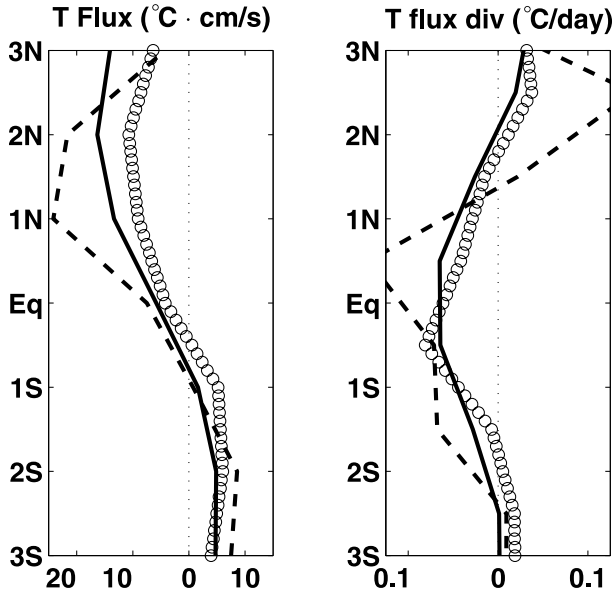

Figure 9. Meridional (a) eddy temperature flux and (b) eddy temperature flux divergence (ETFD) for the central and eastern equatorial Pacific using Reynolds' stress estimates from HP (dashed line), spline-removed Reynolds' stress estimates (solid line), and parameterized estimates (open circles) using $\hat{\kappa}_v = 9.1 \times 10^7$ cm^2/s as determined from calculations based on the eddy mean flow decomposition used throughout the study.

referred to as HP). It is also a region characterized by complicated mean flow and nonstationarity where estimates of diffusivities have proved difficult. The ETFD estimated by Reynolds stress statistics provides a standard of comparison for the eddy diffusivity estimates computed in this study. Moreover, in this region, previous estimates have been computed that provide a historical comparison with the results of the present analysis [e.g., *Swenson and Hansen*, 1999; HP].

7.1. Direct Estimates of ETFD Using Reynolds Stresses

[71] Reynolds stress estimates of ETFD are obtained from meridional eddy velocities. The divergence of the meridional temperature flux is $\mathrm{d}\langle v'T'\rangle/\mathrm{dy}$. The region of interest is located in the eastern equatorial Pacific Ocean between 130°W and 100°W in the equatorial waveguide, (3°S to 3°N). The meridional eddy velocity, v', is estimated from the eddy mean decomposition using the splining method of B98. Similar application of this splining method is used to estimate the mean temperature $\langle T_{spl}\rangle$ and the residuals (deviations), T'. Reynolds temperature flux, $\langle v'\mathrm{T}'\rangle$, is estimated and the meridional gradient is computed from 1° latitude bins. The results of the Reynolds stress estimates of ETFD are shown in Figure 9b. Northward velocity departures (v') are associated with negative temperature departures (T') between about 2°S and 2°N and hence the covariance between v' and T' is negative. Recalling that a mean meridional Ekman divergence upwells cool water along the equator, negative $\langle v'\mathrm{T}'\rangle$ implies a northward eddy flux of cooler water from the equator.

7.2. Eddy diffusivity Parameterization

[72] Eddy temperature flux divergence estimates obtained from the eddy diffusivity parameterization is formulated by the following equation

$$ETFD = -\nabla \cdot (\kappa \nabla \langle T \rangle) \tag{10}$$

where $\langle T\rangle$ is the mean SST (or mixed layer depth) temperature, κ is the eddy diffusivity estimate and ∇ is the horizontal differential operator. For constant eddy diffusivity, the meridional component of the temperature flux is: $-\left(\kappa_v \frac{\partial^2 \langle T\rangle}{\partial y^2}\right)$. The estimate of $\hat{\kappa}_v$ is computed from the eddy mean flow decomposition method as used throughout this study and its value for the eastern equatorial Pacific region (EqE) is $\hat{\kappa}_v = 9.1 \times 10^7$ cm^2/s. The meridional temperature gradient is obtained from the splined mean temperature field by zonal averaging (130°W to 100°W) in 1° latitude bins and then computing 1° meridional differences. These estimates of ETFD compare well with the direct Reynolds stress calculation in Figure 9, where the parameterization (equation 10) slightly underestimates(overestimates) the temperature flux north(south) of the equator.

7.3. Comparison With Earlier Study

[73] HP computed momentum and temperature flux estimates from the observations of 20 satellite-tracked surface drifters during the active TIW season (June 6 through October 27, 1979) in the equatorial and near-equatorial region 130°W to 100°W and 9°S to 7.5°N. Their maximum meridional temperature flux occurred near 2°N with equatorward (negative) values of 28°C cm/s (Figure 9).

[74] Eddy temperature flux and ETFD estimates were computed from Reynolds stresses (HP and the spline-removed residuals ($\langle v'_{spl}T'_{spl}\rangle$)) and the parameterization using $\hat{\kappa}_v$ and $\langle T_{spl}\rangle$ (equation 10). Maximum temperature flux near 2°N occurs for all three estimates however, the values obtained by HP are nearly twice our parameterized values. The spline-removed residuals $\langle v'_{spl}T'_{spl}\rangle$ lie between the other two estimates (Figure 9a). HP emphasize that their sampling density was small and the 1979 TIW season may have been anomalously strong, suggesting that their larger estimates may not be typical. The lower magnitudes and "smoothness" of the Reynolds' stress estimate $\langle v'_{spl}T'_{spl}\rangle$ derived herein are a consequence of increased sampling density and possibly interannual variability.

[75] Within 2° of the Equator, the three estimates of ETFD (Figure 9b) are comparable although that obtained from the HP analysis are generally larger in magnitude. Further, longitudinal averaging over 30° to compute a mean meridional temperature profile may act to dampen the maximum negative ETFD in the equatorial band using the parameterized ETFD (equation 10) compared to the direct method.

8. Conclusions

[76] Eddy diffusivity estimates have been derived from the Equatorial Pacific Ocean Climate Study (EPOCS) and the Tropical Ocean-Global Atmosphere (TOGA) Lagrangian surface drifting buoy data sets for the tropical Pacific Ocean. The data span the years 1979 through mid-1996 and

have been analyzed with the eddy-mean decomposition method used by B98. One of the main difficulties in estimating diffusivity stems from the fact that the simple Taylor definition (1) does not apply in the presence of inhomogeneity and nonstationarity. To address this problem, a preliminary analysis has been performed in order to identify space and time subsets of data where the eddy statistics can be considered approximately homogeneous and stationary. The B98 methodology has then been applied to each subset in order to properly identify the space dependent mean field, $\hat{\mathbf{U}}(\mathbf{x})$, and the associated eddy residual, $\hat{\mathbf{u}}'$, from which diffusivity, $\hat{\kappa}$, is computed.

[77] Zonal and meridional estimates of eddy diffusivity were presented for ten regions and for mostly 3 month temporal partitions (Figure 5). Although zonal diffusivity estimates vary with latitude from about 5×10^7 to 73.5×10^7 cm^2/s (more than one order of magnitude), meridional diffusivity estimates are characterized by low values and small variability (ranging from ≈ 2 to 9×10^7 cm^2/s). A similar anisotropy is not found in the variance values, which are of the same order for both components. To aid in describing and interpreting these results, a conceptual framework in terms of simple stochastic models of turbulence has been introduced.

[78] Away from the equator, where the eddy variance is relatively low, zonal and meridional statistics are found to be approximately described by a first-order autoregressive (AR(1)) model with an exponentially decaying autocorrelation. Small deviations from the AR(1) model are observed, likely related to intermittent inertial oscillations. These results are qualitatively similar to results of a number of previous works obtained in various ocean surface regions [e.g., *Krauss and Böning*, 1987; *Figueroa and Olson*, 1989; *Falco et al.*, 2000]. The AR(1) description is a highly idealized model of turbulence [e.g., *Yaglom*, 1962], valid for random processes in the absence of coherent structures. Despite its simplicity, the AR(1) model appears to provide an acceptable description of surface transport processes, at least in regions where the variability is not highly affected by coherent structures such as waves or vortices.

[79] A different situation is found in regions near the equator, characterized by strong wave activity (NE, EqE, EqW in Figure 1). Here, while the zonal component can still be characterized by an AR(1) process, the meridional component shows significantly different characteristics. In particular, the autocovariance is characterized by a significative negative lobe, suggestive of a second-order (AR(2)) process. Even though the zonal and meridional variances, $\hat{\sigma}^2$, are similar, the difference in the autocovariance structures leads to a strong anisotropy in the diffusivities, with the meridional diffusivity being almost one order of magnitude smaller than the zonal one (see Figures 6 and 7). Technically, this is due to the fast decay and the negative lobe in the meridional autocovariance. Physically, the asymmetry can be understood considering the suggestion of *Flament et al.* [1996], that the TIW transport is carried out by finite amplitude disturbances drifting westward along the sheared SEC and NECC, rather than by a purely linear wave process. The corresponding particle trajectories are cycloidal, with the meridional motion dominated by oscillations (AR(2)-like process), while the zonal motion is primarily characterized by the westward drift (AR(1)-like process). Oscillating wave motion, being coherent at initial time lags, leads to a substantial initial particle displacement, (related to the high variance), followed by a partial return. The actual dispersion, therefore, is much lower than what is suggested by the initial displacements and by the eddy variance.

[80] By plotting κ versus σ^2 for the obtained estimates (Figure 8), the difference between the AR(1) and AR(2) processes is highlighted. The zonal and meridional off-equatorial diffusivities, approximately modelled as AR(1) processes, increase as the eddy variances increase, indicating that the integral timescale, $T_L = \kappa/\sigma^2$, has a nearly constant value, $T_L \approx 5$ days. The meridional AR(2)-like diffusivities of the equatorial regions, instead, appear nearly constant while eddy variances, associated with wave motion, increase.

[81] Further, an independent confirmation of the diffusivity estimates in the central and eastern Pacific was obtained by comparing tracer flux divergence computed from a parameterization using diffusivity estimates of our analysis and that from direct eddy Reynolds stress flux divergence. Although this region is known for its inhomogeneous and nonstationary flows, the diffusivity estimated in this study is consistent with the eddy temperature flux divergence (ETFD) computed directly from our data as well as with estimates derived by others [*Swenson and Hansen*, 1999; HP].

[82] In summary, the eddy mean flow decomposition presented here allows for the computation of fundamental turbulence parameters such as diffusivity, κ, and the Lagrangian integral timescale, T_L, in the equatorial regions, despite the heavy influence of inhomogeneity, nonstationarity and coherent wave structures. Computing these quantities, and in particular diffusivities, is of great relevance for climate studies, since they can be used as guidance for low resolution climatic models where the eddy field is not correctly resolved. In addition to this, the study introduces a simple conceptual framework to interpret the different eddy statistics and the transport parameters found in off-equatorial and near equatorial regions.

[83] The present work still has a number of limitations that can be addressed and pursued in future work. First, as shown in Figure 6, diffusivity estimates are not presently available for all the space and time subsets. In some cases, the diffusivity, $\hat{\kappa}$, has not been found to asymptote, because of poor sampling and/or especially high nonstationarity. Estimates might be improved in the future, using a larger data set. Also, an important issue of great importance in the tropical regions that has not been addressed here is the role of interannual variability. As the data set grows with continued deployments of surface drifters, it will be important in the study of climate to revisit this analysis, resolving variability at interan timescales.

[84] Finally, in the present work, we have suggested the use of first-order and second-order stochastic models to describe eddy statistics in various ocean regions, depending on the relative importance of coherent structures in the eddy field. These models represent the simplest possible choice to provide a qualitatively reasonable description of the observed turbulent processes. Notice though that other, more sophisticated, alternatives are possible, especially for transport in the presence of coherent structures, as recently

suggested by other authors. *Berloff and McWilliams* [2002] have proposed the use of higher-order autoregressive models, based on the analysis of numerical trajectories in a simplified ocean model, while *Pasquero et al.* [2001] have suggested the use of a two-process stochastic model based on 2-D turbulence results. Also, recent works in atmospheric turbulence [*Reynolds*, 2002] suggest the use of low-order stochastic models with "spin". A comparison and a quantitative validation of these different hypotheses will be possible in future work with a more extensive data set.

[85] **Acknowledgments.** The authors would like to thank A. Mariano, D. Olson, C. Rooth and D. Mayer for comments, discussion and invaluable insight. M.S.S. was supported in part by the NOAA/OGP Pan American Climate Study. S.B. and A.G. were supported by 2 ONR grants, N00014-91-J-1346 and N00014-97-1-0620 and AOML/NOAA during the writing of the manuscript.

References

Bauer, S., Eddy-mean flow decomposition and eddy-diffusivity estimates in the tropical Pacific Ocean, Ph.D. diss., Univ. of Miami, Miami, Fla., 2000.

Bauer, S., M. S. Swenson, A. Griffa, A. J. Mariano, and K. Owens, Eddy-mean flow decomposition and eddy-diffusivity estimates in the tropical Pacific Ocean, 1, Methodology, *J. Geophys. Res.*, *103*, 30,855–30,871, 1998.

Berloff, P. S., and J. C. McWilliams, Material transport in oceanic gyres, part 2. Hierarchy of stochastic models, *J. Phys. Oceanogr.*, *32*, 797–830, 2002.

Bi, K., Variability of the surface layer circulation in the western equatorial Pacific, Ph.D. diss., Univ. of Calif., San Diego, 1995.

Borgas, M. S., T. Flesch, and B. L. Sawford, Turbulent dispersion with broken reflexional symmetry, *J. Fluid Mech.*, *332*, 141–156, 1997.

Davis, R. E., Modeling eddy transport of passive tracers, *J. Mar. Res.*, *45*, 635–666, 1987.

Davis, R. E., Observing the general circulation with floats, *Deep Sea Res., Part A*, *38*, Suppl. 1, S531–S571, 1991.

Falco, P., A. Griffa, P. M. Poulain, and E. Zambianchi, Transport properties in the Adriatic Sea as deduced from drifter data, *J. Phys. Oceanogr.*, *30*, 2055–2071, 2000.

Figueroa, H. A., and D. B. Olson, Lagrangian Statistics in the South Atlantic as derived from SOS and FGGE drifters, *J. Mar. Res.*, *47*, 525–546, 1989.

Flament, P. J., S. C. Kennan, R. A. Knox, P. P. Niiler, and R. L. Bernstein, The three-dimensional structure of an upper ocean vortex in the tropical Pacific Ocean, *Nature*, *383*, 610–613, 1996.

Frankignoul, C., F. Bonjean, and G. Reverdin, Interannual variability of surface currents in the tropical Pacific during 1987–1993, *J. Geophys. Res.*, *101*, 3629–3647, 1996.

Griffa, A., Applications of stochastic particle models to oceanographical problems, in *Stochastic Modeling in Physical Oceanography*, edited by R. Adler, P. Muller, and B. Rozovskii, pp. 114–140, Birkhäuser, Boston, 1996.

Hansen, D. V., and C. A. Paul, Genesis and effects of long waves in the equatorial Pacific, *J. Geophys. Res.*, *89*, 10,431–10,440, 1984.

Krauss, W., and C. W. Böning, Lagrangian properties of eddy fields in the northern North Atlantic as deduced from satellite-tracked buoys, *J. Mar. Res.*, *45*, 259–291, 1987.

Legeckis, R., Long waves in the eastern equatorial ocean: A view from a geostationary satellite, *Science*, *197*, 1179–1181, 1977.

Niiler, P. P., A. S. Sybrandy, K. Bi, P.-M. Poulain, and D. S. Bittermam, Measurements of the water-following capability of holey-sock and TRISTAR drifters, *Deep Sea Res., Part I*, *42*, 1951–1964, 1995.

Pasquero, C., A. Provenzale, and A. Babiano, Parameterization of dispersion in two-dimensional turbulence, *J. Fluid Mech.*, *439*, 279–303, 2001.

Philander, S. G. H., *El Niño, La Niña, and the Southern Oscillation*, Academic, San Diego, Calif., 1990.

Priestley, M. B., *Spectral Analysis and Time Series*, Academic, San Diego, Calif., 1981.

Ralph, E. A., K. Bi, P. P. Niiler, and Y. du Penhoat, A Lagrangian description of the western equatorial Pacific response to the wind burst of December 1992: Heat advection in the warm pool, *J. Clim.*, *10*, 1706–1721, 1997.

Reverdin, G., C. Frankignoul, E. Kestenare, and M. J. McPhaden, Seasonal variability in the surface currents of the equatorial Pacific, *J. Geophys. Res.*, *99*, 20,323–20,344, 1994.

Reynolds, A. M., On the dynamical content of Lagrangian stochastic models in h well-mixed class, *Boundary Layer Meteorol.*, *103*, 143–162, 2002.

Rossby, H. T., S. C. Riser, and A. J. Mariano, The western north Atlantic—A Lagrangian viewpoint, in *Eddies in Marine Science*, edited by A. R. Robinson, Springer-Verlag, New York, 1983.

Stammer, D., Global characteristics of ocean variability estimated from regional TOPEX/Poseidon altimeter measurements, *J. Phys. Oceanogr.*, *27*, 1743–1769, 1997.

Swenson, M., and D. V. Hansen, Tropical Pacific Ocean mixed layer heat budget: The Pacific cold tongue, *J. Phys. Oceanogr.*, *29*, 69–81, 1999.

Taylor, G. I., Diffusion by continuous movements, *Proc. London Math. Soc.*, *20*, 196–212, 1921.

Thomson, D. J., Criteria for the selection of stochastic models of particle trajectories in turbulent flows, *J. Fluid Mech.*, *180*, 529–556, 1987.

Yaglom, A. M., An Introduction to the Theory of Stationary Random Functions, Prentice-Hall, Englewood Cliffs, N. J., 1962.

S. Bauer, Atlantic Oceanographic and Meteorological Laboratory, National Oceanic and Atmospheric Administration, Miami, FL 33149-1097, USA.

M. S. Swenson, Fleet Numerical Meteorology and Oceanography Center, Monterey, California, USA.

A. Griffa, Istituto Studio Oceanografia Fisica, Consiglio Nazionale Ricerche, La Spezia, Italy.